

A Six Planet Resonance Chain in K2-138?

M. CERIONI¹ AND C. BEAUGÉ¹

¹*Instituto de Astronomía Teórica y Experimental (IATE),
Observatorio Astronómico, Universidad Nacional de Córdoba,
Laprida 854, (X5000BGR) Córdoba, Argentina*

ABSTRACT

The K2-138 system hosts six planets and presents an interesting case study due to its distinctive dynamical structure. Its five inner planets are near a chain of 3/2 two-body mean-motion resonances, while the outermost body (planet g) is significantly detached, having a mean-motion ratio of $n_f/n_g \sim 3.3$ with its closest neighbor. We show that the orbit of m_g is actually consistent with the first-order three-planet resonance (3P-MMR) characterized by the relation $2n_e - 4n_f + 3n_g = 0$ and is the first time a pure first-order 3P-MMR is found in a multi-planet system and tied to its current dynamical structure. Adequate values for the masses allow to trace the dynamical history of the system from an initial capture in a 6-planet chain (with n_f/n_g in a 3/1 resonance), up to its current configuration due to tidal interactions over the age of the star. The increase in resonance offset with semi-major axis, as well as its large value for n_f/n_g can be explained by the slopes of the pure three-planet resonances in the mean-motion ratio plane. The triplets slide outward over these curves when the innermost pair is pulled apart by tidal effects, in a *pantograph*-like manner. The capture into the 3P-MMR is found to be surprisingly robust given similar masses for m_g and m_f , and it is possible that the same effect may also be found in other compact planetary systems.

Keywords: Exoplanets (498) — Orbital resonances (1181)

1. INTRODUCTION

One of the things we learnt from the *Kepler Space Telescope* is about the significant lack of 2-planet mean-motion resonances (2P-MMRs) among low-mass planets ($< 20m_\oplus$) when compared to their high-mass counterparts ($> 100m_\oplus$) (Lissauer et al. 2011; Winn & Fabrycky 2015). Nevertheless, we still find rich resonant dynamics in the former domain.

On one hand, it has been recently argued that, even when lacking in *pair*-wise commensurabilities, their distribution of orbital periods shows a correlation with the web of 3-planet mean-motion resonances (3P-MMRs) (Cerioni et al. 2022), suggesting a more complex resonant evolution than previously thought. On the other hand, planetary systems showing a high number of MMRs among its constituents are predominantly low-mass (e.g Kepler-60, Kepler-80, Kepler-223, TRAPPIST-1, TOI-178, K2-138, etc.), although some examples are also found in systems harboring massive

planets (e.g. GJ876 and HR8799). These multi-resonant systems appear as "resonance chains" with multiple links of adjacent 2P-MMRs and (consequently or not) zero-order 3P-MMRs.

We do not expect these commensurabilities to be the outcome of *in-situ* formation with fortunate initial conditions. That scheme falls short because it fails to account for the meaningful gravitational interactions between planetesimals and a gaseous protoplanetary disk, mainly, disk-induced migration. This mechanism is characterised by a smooth decrease in semi-major axis, forcing a slow inward spiraling of the bodies towards the star.

Depending on their relative rates, migration can lead two planets into a resonance. Although in the case of divergent migration (where planet separation increases) planets are unlikely to become trapped in resonance (e.g, Henrard & Lemaître 1983), the case of convergent migration (where planet separation decreases) is different. Convergent migration can lead to permanent capture into resonance (Goldreich & Tremaine 1980; Lee & Peale 2002), and is believed to be the cause of most observed MMRs, such as that of Neptune and Pluto (Malhotra

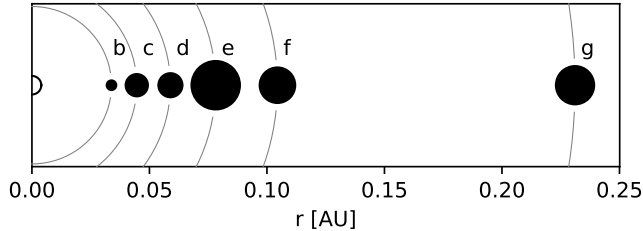


Figure 1. Sketch of K2-138. The white circle on the left corresponds to the central star. The solid lines correspond to their semi-major axes as listed in Table 1. Black dot sizes are proportional to the measured radii.

1991), the satellites of Jupiter and Saturn, as well as several large-mass exoplanetary systems (e.g., Lee & Peale 2002; Beaugé et al. 2003; Ramos et al. 2017).

It is believed that resonance capture in stable solutions of first-order MMRs is highly probable provided sufficiently slow smooth differential migration and low initial eccentricities (see Henrard & Lemaître 1983; Beaugé et al. 2006; Batygin 2015). Resonance chains are therefore expected to be a frequent outcome given any system of multiple migrating low-mass planetesimals, although many may succumb under instabilities induced by the other planets and disrupt after disk dispersal (e.g., Thommes et al. 2008; Lega et al. 2013; Izidoro et al. 2017).

One resonant system that recently caught our attention is K2-138, the first K2 system discovered by citizen scientists through the Exoplanet Explorers program on the Zooniverse platform (Christiansen et al. 2018).

K2-138 is a K-Dwarf type star with mass $m_0 = 0.93 \pm 0.02 m_\odot$ and radius $R_0 = 0.86 \pm 0.03 R_\odot$, hosting one super-Earth and five sub-Neptunes (Christiansen et al. 2018; Lopez et al. 2019; Hardegree-Ullman et al. 2021). A sketch of the system’s architecture can be seen in Figure 1. In addition to the Kepler lightcurves, HARPS radial velocity measurements and Spitzer lightcurves have allowed to simultaneously constrain planetary orbits, radii and (in some cases) masses. The complete list of K2 and HARPS derived planetary parameters are presented in Table 1.

As we can see, its architecture is characterised by five tightly packed inner planets separated by a significant gap from m_g . Relative separations, as described by mean-motion ratios between adjacent planets, are $n_b/n_c = 1.513$, $n_c/n_d = 1.518$, $n_d/n_e = 1.529$, $n_e/n_f = 1.544$ and $n_f/n_g = 3.290$. We use these values in Figure 2 to locate adjacent planetary triplets in the space of mean-motion ratios, where we can study their proximity to different resonances (vertical and horizon-

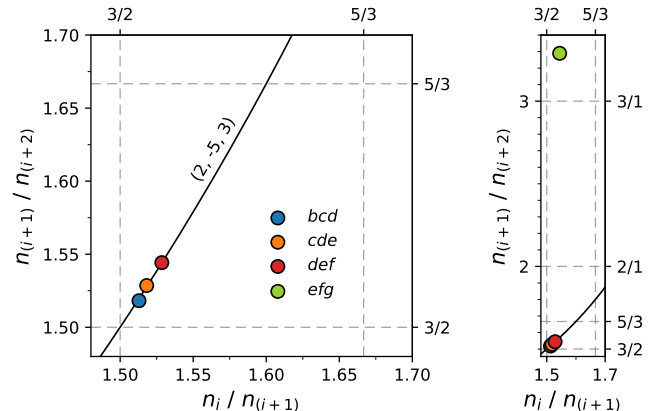


Figure 2. Mean-motion ratio plane for K2-138. Colored dots correspond to each set of three adjacent planets (triplets). The x -axis corresponds to the mean-motion ratio between the innermost and middle planet, while the y -axis is for middle and outermost. Dashed vertical and horizontal lines correspond to 2P-MMRs, while the diagonal solid line corresponds to the $(2,-5,3)$ 3P-MMR. Given the large separation of $n_f/n_g \sim 3.29$, the efg triplet is shown in the **right frame**.

tal dashed lines for 2P-MMRs ; diagonal solid lines for 3P-MMRs).

A few different features immediately stand out. The five inner planets are located near an intersection of 2P-MMRs, suggesting a 5-planet chain of consecutive near first-order $3/2$ MMRs and the longest $3/2$ chain known to date. The green dot, corresponding to the efg triplet, is separated from the rest because of the notoriously large gap between m_f and m_g . In addition, the inner triplets are located on top of the zero-order $(2,-5,3)$ 3P-MMR, plotted as the solid black line. Lastly, we note that the offsets which separate the planets from the exact $3/2$ intersection interestingly increase with the distance to the star.

The dynamical history which led K2-138 to its current configuration remains uncertain from several angles. For instance: Could the inner planets truly be in a 5-planet $3/2$ resonance chain in spite of their sizable offsets? The origin of the gap between m_f and m_g is also unclear. Why is the sixth planet so isolated from the rest given that all underwent a similar migration process? Is it really detached from the inner resonance chain?

Both Lopez et al. (2019) and Hardegree-Ullman et al. (2021) speculate about two non-transiting planets at ~ 19 and ~ 30 days, which would complete an 8-planet chain of $3/2$ MMRs and help explain the current location of m_g . However, this is not the only hypothesis.

Considering only the confirmed planets so far, it is not obvious whether m_f is detached from the inner chain or not. It is possible that during the migration process m_g

Table 1. K2-138 planetary parameters as derived and presented in Lopez et al. (2019).

Planets	P (days)	a (AU)	e	R (R_{\oplus})	m (m_{\oplus})
b	$2.35309^{+0.00022}_{-0.00022}$	$0.03385^{+0.00023}_{-0.00029}$	$0.048^{+0.054}_{-0.033}$	$1.510^{+0.110}_{-0.084}$	$3.1^{+1.1}_{-1.1}$
c	$3.56004^{+0.00012}_{-0.00011}$	$0.04461^{+0.00030}_{-0.00038}$	$0.045^{+0.051}_{-0.032}$	$2.299^{+0.120}_{-0.087}$	$6.3^{+1.1}_{-1.2}$
d	$5.40479^{+0.00021}_{-0.00021}$	$0.05893^{+0.00040}_{-0.00050}$	$0.043^{+0.041}_{-0.030}$	$2.390^{+0.104}_{-0.084}$	$7.9^{+1.4}_{-1.3}$
e	$8.26146^{+0.00021}_{-0.00022}$	$0.07820^{+0.00053}_{-0.00066}$	$0.077^{+0.048}_{-0.049}$	$3.390^{+0.156}_{-0.110}$	$13.0^{+2.0}_{-2.0}$
f	$12.75758^{+0.00050}_{-0.00048}$	$0.10447^{+0.00070}_{-0.00088}$	$0.062^{+0.064}_{-0.043}$	$2.904^{+0.164}_{-0.111}$	< 8.69
g	$41.96797^{+0.00843}_{-0.00725}$	$0.23109^{+0.00154}_{-0.00196}$	$0.059^{+0.063}_{-0.040}$	$3.013^{+0.303}_{-0.251}$	< 25.47

was captured in a 3/1 MMR with m_f , and the large observed resonance offset (~ 0.3) is either primordial or a consequence of dynamical evolution after the dispersal of the protoplanetary disk. In such a case, all six planets would have formed a complete resonance chain, at least at some point of their history.

While this idea is intriguing, it is unclear how such a large offset may have been achieved. There are two main processes which are frequently invoked to explain deviations from an observed mean-motion ratio with respect to the nominal resonant value: differential migration in a flared-disk (Ramos et al. 2017) and tidal effects (e.g. Lithwick & Wu 2012; Delisle & Laskar 2014). Although these effects are dependent on the masses, in both scenarios the offset is expected to decrease with larger semi-major axis, contrary to what is observed. Moreover, the observed mean-motion ratio between the two outermost planets appears notoriously large, particularly for a second-order resonance where the family of zero-amplitude solutions deviate only slightly with respect to the exact resonance position.

In this work, we study the cases of both a detached (non-resonant) and an attached (resonant) outermost planet m_g and test under which conditions each may have occurred. Section 2 describes the migration framework as well as the protoplanetary disk adopted for our N-body simulations of Type-I migration. Section 3 estimates the necessary masses for the two outermost planets leading to the detached or attached configurations. In Section 4 we discuss the first possibility: a 5-planet resonance chain $m_b - m_f$ plus the outermost planet m_g as a non-resonant distant companion. Section 5 focuses on the second option and analyses how very large resonance offsets may be achieved in multi-resonant systems. In both scenarios we analyze what would be the necessary planetary masses and disk parameters to reproduce the observed dynamical features and how robust these solutions are likely to be. Finally, the *pantographic effect* leading to increasing offsets is explained in detail in Sec-

tion 6, while a general discussion and future prospects close the paper in Section 7.

2. PLANETARY MIGRATION

2.1. Migration Scheme

The gravitational interaction between a low-mass planet and a protoplanetary disk results in orbital decay, usually known as Type-I planetary migration. An analytical prescription was originally developed by Tanaka et al. (2002), who considered a single fully formed planet in a circular orbit and a three-dimensional isothermal gaseous disk with a surface density Σ and aspect ratio H given by

$$\Sigma(r) = \Sigma_0 \left(\frac{r}{r_0} \right)^{-s}, \quad H(r) = H_0 \left(\frac{r}{r_0} \right)^f, \quad (1)$$

where s and the disk flare index f characterise the surface density distribution and shape of the disk, respectively. If $f = 0$, the disk profile is linear (flat), while $f > 0$ describes a curved (flared) disk. Both (Σ_0, H_0) are the values at $r_0 = 1$ au.

The expression for the orbital decay τ_a was proposed by Tanaka et al. (2002) for the case described. Later on, Tanaka & Ward (2004) extended the model for planets in eccentric orbits, which would circularize when embedded in a disk. The expressions for both the migration and circularization timescales are given by

$$\tau_a \equiv \left| \frac{a}{\dot{a}} \right| = \frac{Q_a t_w}{H(r)^2}; \quad \tau_e \equiv \left| \frac{e}{\dot{e}} \right| = Q_e \frac{t_w}{0.78} \quad (2)$$

where $Q_a^{-1} \simeq 2.7 + 1.1s$ and we assume the ad-hoc eccentricity damping factor adopted by Cresswell & Nelson (2006) of $Q_e = 0.1$. Lastly, t_w is the wave timescale given by

$$t_w = \frac{m_0}{m_p} \frac{m_0}{\Sigma(r)r^2} \frac{H(r)^4}{\Omega_K(r)}, \quad (3)$$

where m_p is the mass of the planet under consideration and m_0 the mass of the star. The Keplerian angular velocity is given by $\Omega_K(r) = \sqrt{G(m_0 + m_p)/r^3}$. Note that

equations (2) and (3) show that the migration velocity is directly proportional to the planetary mass, as well as dependent on the disk parameters. Thus, the mass distribution in a given system is largely responsible for the convergence or divergence between two or more planets, as well as the possibility of resonance trapping (see Beaugé & Cerioni 2022).

In order to account for the coupling between semi-major axis and eccentricities during the migration process, Goldreich & Schlichting (2014) modified expressions (2) with a β factor to quantify the conservation on the angular momentum. The effective timescale for the radial drift is

$$\frac{1}{\tau_{a_{\text{eff}}}} = \frac{1}{\tau_a} + 2\beta \frac{e^2}{\tau_e}. \quad (4)$$

When $\beta = 0$ there is no coupling while $\beta = 1$ implies no loss in the orbital angular momentum. Goldreich & Schlichting (2014) suggest $\beta = 0.3$ following estimations by Tanaka & Ward (2004).

2.2. Disk Parameters

For our N-body simulations and analytical estimates we assumed a thin laminar flat disk ($f = 0$) characterized by a surface density exponent of $s = 1/2$ and an aspect ratio of $H_0 = 0.05$ at $r_0 = 1$ au. We considered several values of the surface density Σ_0 from 100 up to 1700 gr cm^{-2} . In most cases we observed no significant difference in the outcome.

These parameters were chosen for the sake of simplicity considering our lack of information of the real disk. At the very least, we expect our results to be robust with respect to reasonable variations of the disk parameters. Equations (2) and (3) show that τ_a is directly proportional to H_0 , and inversely so to s , f , and Σ_0 ; we can therefore predict the evolution timescale and necessary integration time of our simulations as a function of these parameters.

While the general trend of the migrating system is expected to be fairly robust to disk parameters, the conditions of resonance capture and the subsequent orbital evolution of the resonance chain may be more sensitive. For this reason, each new set of parameters led to a new calculation of capture conditions with our analytical model and new N-body simulations. More details will be given in the next section.

3. MASS ESTIMATES FOR DETACHMENT

As may be seen in Table 1, even if fairly reasonable estimations of planetary masses are available for the first four planets, only upper bounds are given for the two outermost bodies. Beaugé & Cerioni (2022) showed that the formation of a resonance chain is particularly sensitive to the mass of the last (and first) planet, so the

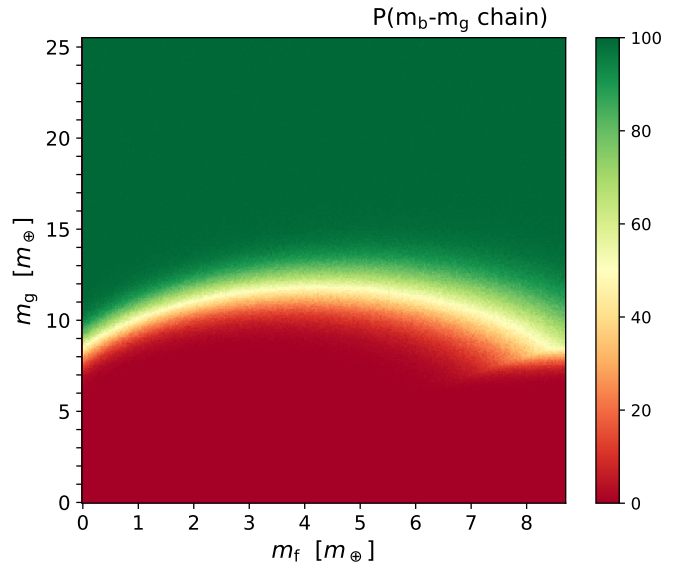


Figure 3. Percentage of fictitious 6-planet systems $m_b - m_g$ that lead to global convergent migration and the formation of a complete resonance chain. While m_f and m_g are varied in a regular grid, for each cell the values of the other masses are drawn from a PDF consistent with Table 1.

estimation of (m_f, m_g) can provide detachment regimes for the sixth planet.

In that spirit, we start by checking which combination of masses would produce a complete 6-planet MMR chain. This calculation does not require N-body simulations but may be undertaken using an analytical resonant capture condition for N planets developed by Beaugé & Cerioni (2022). Truth be said, this method only checks whether a given (e.g. current) distribution of orbital separations is an attractor under the effects of the exterior non-conservative force and thus evolves towards more compact configuration, or whether the evolution will tend to disperse the system.

As mentioned earlier, resonance capture conditions are sensitive to the combination of planetary masses, so in Figure 3 we studied a grid of values (m_f, m_g) , where each mass varied between zero and its upper bound. For each pair of values we generated a set of $N_{\text{sys}} = 10^3$ fictitious systems varying the mass of the other planets from a probability distribution function (PDF) consistent with their observed values*. Then, we checked what percentage of N_{sys} led to the formation of a stable res-

* For each planet i with a measured mass of $m_i^{+\Delta_R}_{-\Delta_L}$, we produced a Skew-Normal distribution with median in m_i and such that its integral in the interval $[m_i - \Delta_L, m_i + \Delta_R]$ yields 0.683 (i.e the 68.3%-credibility interval) and used this PDF to draw random masses.

onance chain. The color assigned to each cell represents this ratio.

As shown by the color code on the right, the percentage of positive values (i.e. convergent infall of the complete 6-planet system) varies from zero for low values of $m_g \lesssim 7 m_\oplus$, to mixed values around $m_g \sim 8 - 12 m_\oplus$, to 100% for $m_g \gtrsim 13 m_\oplus$. For the migration of m_g onto the inner system, these three regions respectively represent: i) convergent migration leading to an attached m_g and a 6-planet chain, ii) a mixed domain of slow divergence/convergence, and iii) divergent migration leading to a detached m_g and only an inner 5-planet chain. These limits are only weakly dependent on the adopted value of m_f and the rest of the planets.

We will consider these mass estimates in the following sections in order to analyze two options: an m_g planet which is detached from the inner 5-planet resonance chain, and m_g planet attached to the inner system and forming a complete 6-planet resonance chain.

4. OPTION 1: A 5-PLANET RESONANCE CHAIN

4.1. A Non-Resonant yet Non-Hierarchical m_g

With the innermost planet currently located at $a_b \simeq 0.03$ au around a $0.93 m_\odot$ star, it is fair to say that the planets underwent a large-scale migration from their original formation sites.

In this section we assume a non-resonant sixth planet, which means that for m_g we are avoiding the green region in Figure 3 and considering the red and white areas instead. These are different mass regimes which imply different migration rates. We will take it case by case.

To begin with, if the mass of the outer planet were significantly lower than $7 m_\oplus$ (red tones), then the infall rate of the outermost planet would have been much smaller than that of the resonance chain, leading to a marked hierarchical planetary system with a much larger relative separation than observed. Recall that the mean-motion ratio between the two outer planets is $n_f/n_g \simeq 3.3$ and not too far from the 3/1 MMR.

Therefore, in order to explain the non-resonant but also non-hierarchical location of m_g , the only option is the white-toned region, corresponding to $m_g \sim 8 - 12 m_\oplus$. In this regime, the migration rate of m_g can be slightly smaller or higher than that of the inner resonance chain, leading to a very slow divergent or convergent migration, depending on the particular combination of m_e , m_f , and m_g . The scenario of slow divergence would have seen an early formation of the $m_b - m_f$ chain followed by a slow but persistent increase in the separation with m_g , coming to a halt at the observed separation right at the time of dispersal of the gas disk. The same would be true for the case of a slow convergent

migration of an initially farther out m_g planet cut short before it could reach the 3/1 resonance. While plausible, these alternatives are critically sensitive to the combination of initial separation, disk lifetime and differential migration rates. Nevertheless, given that this section only pretends to study the formation of the inner chain with a non-resonant m_g , we will take its value from this regime.

As a final aside, it is interesting to note that a non-resonant nature for m_g may be proposed as strong evidence against an inner disk edge, or, if present, one that did not play an important role in the migration history of the K2-138 system. If the resonance chain $m_b - m_f$ was stopped at such an edge, then m_g would have ultimately reached its inner companions independently of its mass. Smaller values of m_g would imply longer times, but the outcome would have been the same.

4.2. Planetary Masses

Assuming that the sixth planet will not come into resonance with the inner system, the next question is about the formation of the inner 5-planet chain on its own. In Figure 4 we perform a similar analysis to that of Section 3, this time focusing on which values of m_e and m_f lead to the formation of the inner chain. The values of m_f were varied between zero and the upper bound given in Table 1, while for its inner neighbor we considered values in the range $m_e \in [13 - 2, 13 + 2] m_\oplus$. As before, for each cell of the rectangular grid we generated a series of fictitious systems with the masses of the other planets drawn from a PDF consistent with the observational data.

The formation of the 5-planet resonance chain seems very unlikely for the estimated parameters of the system. As mentioned earlier, the convergence condition is particularly sensitive to the values of the first and last planet in the system (Beaugé & Cerioni 2022). Since the best fit values imply $m_f < m_e$ (even for the upper bound of m_f), convergent migration is highly improbable, especially for m_e larger than its reported median value. The color bar shows some positive results, and with a high probability, but only for $m_e \sim 11 m_\oplus$ and $m_f \simeq 8.5 m_\oplus$. While the outer planet is still less massive than its inner neighbor, an early formation of a resonance chain comprised of $m_b - m_e$ would slow the infall of the inner system sufficiently to allow m_f to catch up and join its kin.

4.3. Initial Separations

A more subtle difficulty in the 6-planet system is related to their initial separation leading to the migration process. Even considering the largest value for m_f and

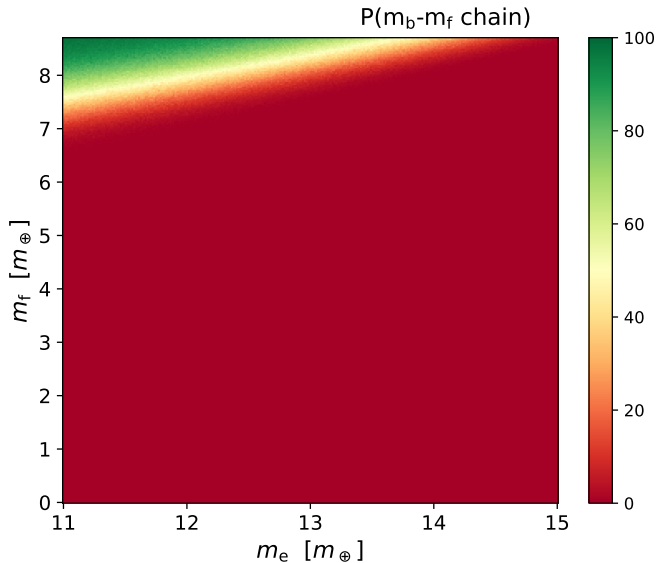


Figure 4. Analogous to Figure 3, but now considering only the 5-planet system comprised of $m_b - m_f$. In both plots the color bars indicates the ratio of systems which converge to a chain.

reasonably low values for m_e (say, $10 m_\oplus$), we still have mass ratios $m_e/m_f \sim 8.69/10 < 1$. From Ramos et al. (2017) we know that the mass ratio between adjacent planets m_i and m_{i+1} leading to 2-planet convergent migration must satisfy the condition

$$\frac{m_{i+1}}{m_i} > \left(\frac{n_i}{n_{i+1}} \right)^{\frac{2}{3}(2f+s-1/2)} \quad (5)$$

where n_i/n_{i+1} is not the resonant mean-motion ratio we wish to achieve but the initial value at the start of the migration. A flat disk ($f = 0$) and a surface density exponent $s = 1/2$ give a minimum value, i.e. $m_{i+1}/m_i = 1$ independent of the initial separation. Other disk parameters, especially those with a steeper surface density, lead to more stringent conditions for the mass ratio.

Since the estimated value of m_e/m_f is smaller than unity, the inner body of the pair migrates faster and m_f lags behind increasing any initial separation. Convergent migration between these two planets is only expected to occur after the inner resonance chain $m_b - m_e$ is established and the effective semi-major axis decay rate is slowed. This behavior is expected for all disk properties and regardless of the initial conditions, although the resulting MMR in which each pair is captured may (and will) vary.

Nevertheless, there is one hard condition on initial separations. Given that the mass ratios of the first four planets is greater than unity, migration is convergent and they will be trapped in a mean-motion commensurability that is lower than their initial separa-

tions. Therefore, we set initial separations greater than $n_i/n_{(i+1)} > 1.5$.

4.4. N-Body Simulations

We performed N-body simulations employing a Bulirsch-Stoer integration scheme with variable time-step and precision $ll = 12$ (Bulirsch & Stoer 1966). All bodies begin with initial separations $n_i/n_{(i+1)} = 1.55$ and migration rates as outlined in 2.1. The left frame of Figure 5 shows results for the aforementioned scenario, where we plot the mean-motion ratio of each adjacent pair of planets as a function of time.

The mass ratio increases subsequently for the first three pairs, so migration is convergent and they rapidly are trapped in a four-planet chain of MMRs. However, since $m_f < m_e$ the fifth planet starts the simulation falling behind and increasing the value of n_e/n_f . This process reverses once the inner system is trapped. The net infall speed of the four-planet chain is now lower than the decay rate of m_f (see Beaugé & Cerioni 2022) and this planet ultimately catches up and joins the resonance chain. No such fate awaits the outermost planet and m_g continues to fall behind increasing its distance with the rest of the pack.

The scenario described above appears consistent with the overall dynamical characteristics of the system, and we were able to obtain similar results for a wide range of disk properties. Variations in the masses also led to analogous results as long as the mass ratios satisfied the convergence/divergence conditions mentioned earlier and outlined in Figures 3 and 4. Different results, however, were found when changing the initial separation between the planets. The central frame of Figure 5 shows a similar N-body simulation as before, but now considering a wider initial system with $n_i/n_{(i+1)} = 1.70$.

Since the planets start the simulation further apart, the migration of the inner pack towards the $3/2$ MMRs takes longer, giving time for m_f to separate even more and encounter a larger number of commensurabilities in its path. When the differential migration reverses, m_f does not reach the $3/2$ MMR with m_e but becomes trapped in the $5/3$, leading to a configuration inconsistent with the one observed. The right frame shows how the final value of the ratio n_e/n_f varies according to the initial separation between adjacent planets.

Unsurprisingly, initial separations close to the $3/2$ MMR yield final systems trapped in such a commensurability and thus analogous to the observed K2-138 6-planet model. However, even slightly wider separations lead to other resonances and other configurations, with the $5/3$ and $2/1$ being the most common, depending on the initial $n_i/n_{(i+1)}$. Although extremely high

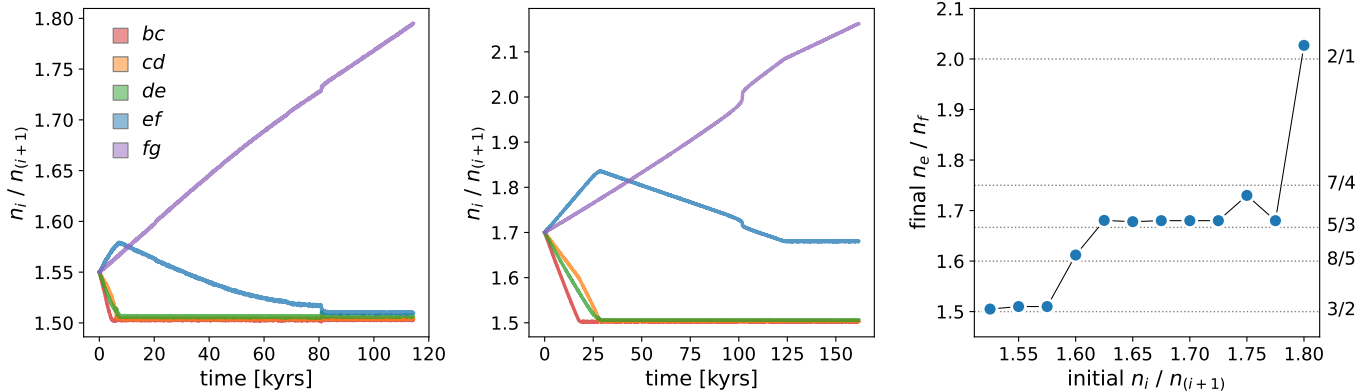


Figure 5. Left Frame: N-body simulations under mutual gravitational perturbations and migration of the 6-planet K2-138 system. Masses were taken equal to $\{m_k\} = (3.1, 6.3, 7.9, 10.0, 8.7, 8.0) m_{\oplus}$, while for the disk parameters we adopted $(s, f, \Sigma_0, H_0) = (0.5, 0, 500 \text{ gr/cm}^2, 0.05)$. All planets were initially placed on circular coplanar orbits with separation such that $n_i/n_{(i+1)} = 1.55$. **Center Frame:** Same as previous plot, but with initial separations equal to $n_i/n_{(i+1)} = 1.70$. **Right Frame:** Final value of n_e/n_f as function of the initial separation.

migration rates will sometimes avoid all these alternate capture sites and fall back to the 3/2, this was rarely the case. The capture condition for a given resonance depends much more strongly on the mass ratio than on the surface density of the disk, and planets with similar masses will suffer similar semi-major axis decay rates even for high values of Σ_0 . We found results analogous to Figure 5 even for $\Sigma_0 = 1700 \text{ gr/cm}^2$, but we did not test higher values.

These simulations seem to indicate that the current 3/2 MMR resonance chain among the five inner planets of K2-138 is possible provided the mass of m_f is close to its upper bound, the mass of m_e is significantly lower than its median value (beyond the 1 or 2 σ -level), and the initial separation between the planets was such that their mean-motion ratios all lied between 1.5 and 1.6. This would require that the planets form around the same time and with very similar mean-motion ratios as those observed today. While all these conditions are, again, possible, they seem to require very fine tuning and some of the parameters (such as the mass ratio m_e/m_f) are very far from the expected values.

5. OPTION 2: A 6-PLANET RESONANCE CHAIN

5.1. The (2,-4,3) 3-Planet Resonance

The idea that the outermost planet (m_g) may form part of the system’s resonance chain is strongly suggested when we analyze the location of the triplet $(n_e/n_f, n_f/n_g)$ in the mean-motion ratio plane. This is shown with a red cross in Figure 6, together with the position of every zero- and first-order (k_1, k_2, k_3) 3P-MMR in the region, with indexes $|k_i| \leq 10$. The 2-planet commensurabilities $n_e/n_f = 3/2$ and $n_f/n_g = 3/1$ are drawn in dashed lines, while 3P-MMRs are shown in

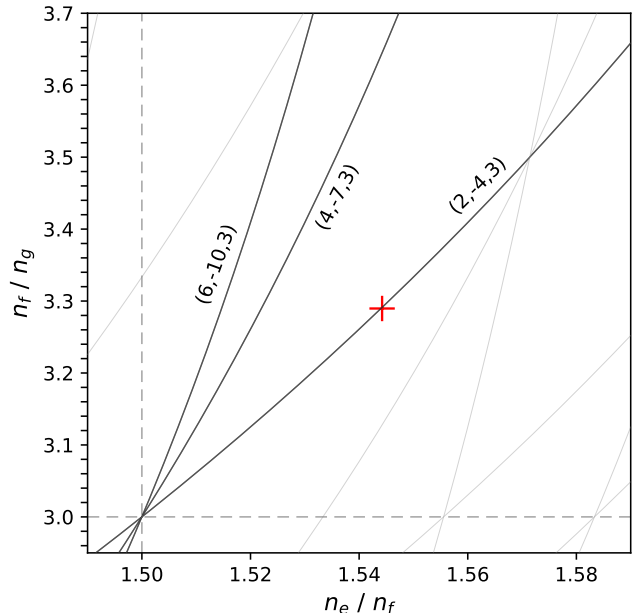


Figure 6. Observed position of the $(n_e/n_f, n_f/n_g)$ triplet (red cross) in the mean-motion ratio space. Diagonal curves mark every low-integer zero- and first-order 3P-MMR that passes through the domain. Commensurabilities crossing the $(3/1, 3/2)$ intersection are labeled and drawn using thicker lines. Error bars are too small to be distinguishable in the figure.

continuous lines. Of these, three resonances cross the $(3/1, 3/2)$ intersection and are highlighted with thicker lines and labeled in the plot.

The location of the three outer planets in this plane is strikingly close to the $(2, -4, 3)$ first-order three-planet resonance, characterized by the relation $2n_e - 4n_f + 3n_g = 0$. Introducing the observed values for the orbital

periods from Table 1, as well as their uncertainties, we obtain

$$2n_e - 4n_f + 3n_g = 0.00020^{+0.00024}_{-0.00015} d^{-1} \quad (6)$$

which comes extremely close to the exact nominal commensurability. Given the limited number of two and three-planets resonances in this region, it seems very unlikely that such a correlation could be a coincidence, even if the 3P-MMR is of first order and thus not the strongest dynamical feature in the vicinity. Similarly to the inner triplets, Figure 6 suggests a capture of $(n_e/n_f, n_f/n_g)$ in the $(3/2, 3/1)$ intersection, with an excursion of the triplet over the three-planet resonance that crosses that intersection.

To prove that the $(2, -4, 3)$ resonance is not only relevant to the current dynamics of the system but also tied to its migration history, we must solve two independent issues: (i) test whether planetary masses consistent with the outer K2-138 system can be trapped in this first-order 3P-MMR and survive the dissipation of the gaseous disk without being expelled from the commensurability, and (ii) explain the large separation of the current configuration with respect to the $(3/2, 3/1)$ intersection of two-planet resonances.

5.2. Formation of the 6-Planet Chain

In principle, there are two possible routes that could lead to the capture of the outer triplet in the $(2, -4, 3)$ resonance; these are divergent and convergent migration.

Divergent migration occurs in a scenario similar to that discussed in the previous section, but with a mass of the outer planet in the range $m_g \lesssim 8m_\oplus$ (Figure 3) and initial separations such that $n_f/n_g < 3$. In the previous section we assumed all planets initially equidistant forming a compact formation; this is not strictly necessary and the outer planet could have began its migration further out. However, we could not find any set of parameters that led to the capture in the $(2, -4, 3)$ three-planet commensurability during divergent migration, so this case is ruled out. As a side note, some cases did result in the zero-order $(4, -7, 3)$ 3P-MMR, with stable orbits and a small but non-zero offset with respect to the two-planet resonances.

We then turn to the second possibility, a convergent migration of m_g from an initial orbit beyond the $3/1$ resonance with m_f in the hope of trapping the three outermost planets in the desired first-order 3P-MMR. As before we fix the masses of the four inner planets to the values chosen in the previous sections: $(m_b, \dots, m_e) = (3.1, 6.3, 7.9, 10.0)m_\oplus$ and with initial separations among adjacent bodies between 1.5 and 1.6.

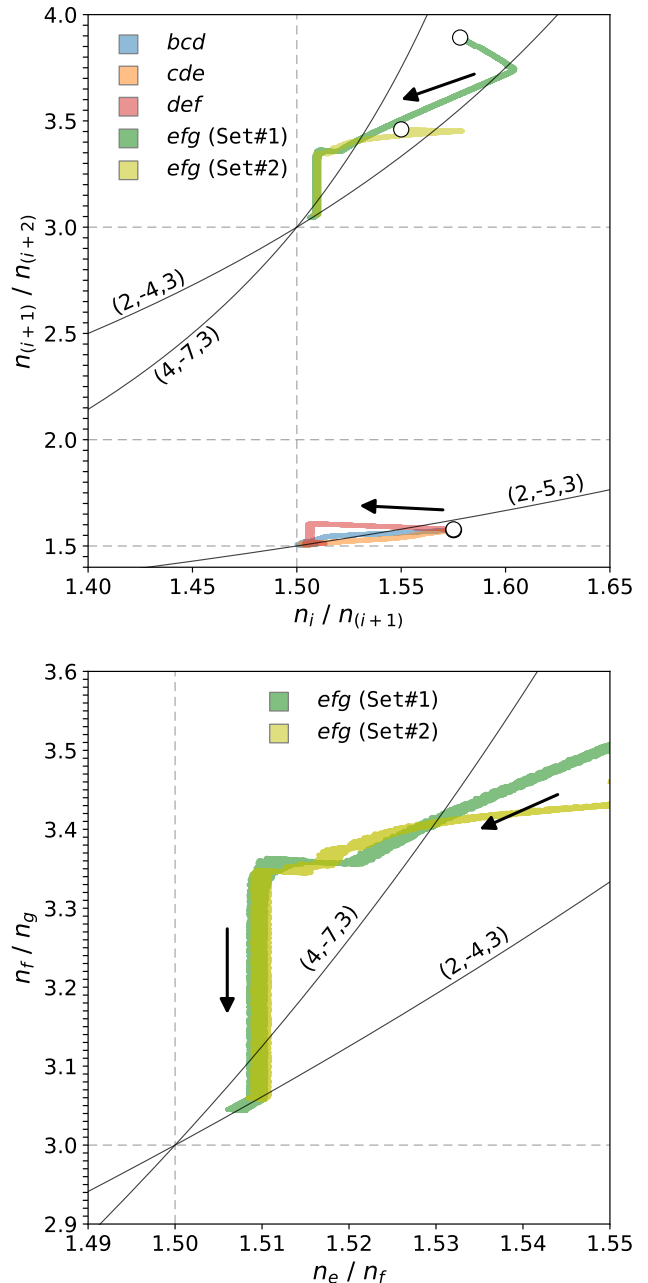


Figure 7. N-body simulations under mutual gravitational perturbations and migration of the K2-138 system in the mean-motion ratio plane. Colored lines correspond to each planetary triplet. Inner triplets belong to **Set#1**, but analogous results are obtained for **Set#2**. The evolution of the efg triplet in both sets are shown in green colors. Initial positions are shown with white circles. Arrows indicate the direction of evolution. **Bottom frame** is a zoom-in of the resting place of the last triplet.

The rest of the masses, as well as their initial separations, and disk parameters were varied.

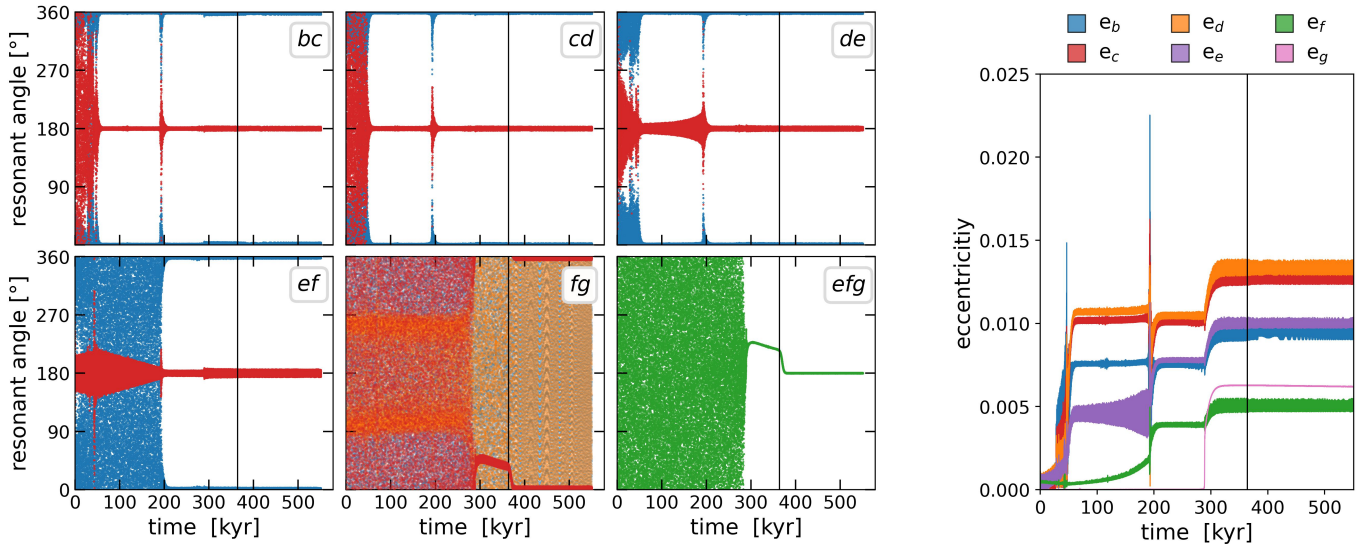


Figure 8. Left Frame: Time evolution of resonant angles corresponding to the simulation **Set#1**. The first four plots on the left show the resonant angles $\sigma_1 = 3\lambda_{i+1} - 2\lambda_i - \varpi_i$ (in blue) and $\sigma_2 = 3\lambda_{i+1} - 2\lambda_i - \varpi_{i+1}$ (in red) for the first four inner planetary pairs (i.e. $i = 1, 2, 3, 4$). The lower center plot shows the resonant angles of the 3/1 MMR between m_f and m_g , where blue is used for $\theta_1 = 3\lambda_g - \lambda_f - 2\varpi_f$, red for $\theta_2 = 3\lambda_g - \lambda_f - \varpi_f - \varpi_g$ and orange for $\theta_3 = 3\lambda_g - \lambda_f - 2\varpi_g$. The capture of the pair into the two-planet resonance is only accompanied by a libration of θ_2 with the other angles circulating. The green data points in the lower-right frame show the time evolution of the resonant angle $\theta_{243} = 2\lambda_e - 4\lambda_f + 3\lambda_g - \varpi_g$ corresponding to the $(2, -4, 3)$ 3P-MMR of the outer triplet. **Right Frame:** Eccentricities of all planets for the same simulation. The disk is smoothly removed from the simulation at $T = 375$ kyr (vertical black line). All subsequent orbital variations occur in a gas-free scenario.

Figure 7 shows the results of two different simulations, labeled **Set#1** and **Set#2**. Their main characteristics are given below:

$$\begin{aligned} \text{Set\#1: } & m_f = 9.3, m_g = 11.0, \Sigma_0 = 100 \text{ g/cm}^2 \\ \text{Set\#2: } & m_f = 8.7, m_g = 8.8, \Sigma_0 = 1000 \text{ g/cm}^2 \end{aligned} \quad (7)$$

where the masses are given in units of m_\oplus . In **Set#1** we tested a value of m_f that is slightly over the reported upper bound as low values of this parameter prevent the formation of the inner chain of multiple 3/2 resonances (Figure 4). Moreover, the mass of the outer planet in **Set#2** was set barely large enough to guarantee convergent migration once the inner system was trapped in its chain. This means a very slow convergent migration w.r.t its inner neighbors and thus its initial semi-major axis could be placed close to the 3/1 MMR with m_f ; we chose $n_f/n_g \simeq 3.4$, although slightly smaller values lead to similar results. Conversely, the mass of m_g in **Set#1** was significantly larger leading to a convergent migration of the outer planet onto m_f even before the resonance lock of the inner system. In consequence the initial separation had to be larger indicative of a more hierarchical primordial system. We opted for $n_f/n_g \simeq 3.8$, although larger values would result in similar final configurations.

The top frame of Figure 7 shows the evolutionary tracks of the mean-motion ratios of all triplets, each

identified with a different color. The large circles indicate the initial values, and arrows show the direction of the evolution. The behavior of the inner system $m_b - m_f$ was similar in both sets, resulting in the formation of the well-known 3/2 resonance chain. The evolution of the outer triplet is shown in green, where a dark tone was chosen for **Set#1**, and a lighter color for **Set#2**.

Both simulations show fairly similar characteristics. Since $m_f < m_e$, initially n_e/n_f increases signaling a divergent migration of this pair. As soon as the inner resonance chain begins to assemble, their migration rate slows and allows m_f to reverse its differential migration. The evolutionary track thus switches direction and the pair $m_e - m_f$ moves towards the 3/2 MMR where it is finally trapped. The behavior of the outer pair is simpler as the value of m_g guarantees convergent migration in both cases. However, while the mass chosen for **Set#1** leads to a relatively fast inward migration from the start of the run, in **Set#2** the outer pair approaches the rest of the system only after the resonance chain begins to form. This explains the almost horizontal evolutionary track during the first part of the simulation.

The bottom frame of Figure 7 zooms in on the vicinity of the final resting place of the outer triplet. After the capture of n_e/n_f in the 3/2 MMR both runs are practically indistinguishable. As the mean-motion ratio of the outer pair n_f/n_g approaches the 3/1 MMR,

it first passes through the $(4, -7, 3)$ 3P-MMR but is finally stopped at the $(2, -4, 3)$ commensurability. Even though this first-order resonance should have a lower capture probability than its near neighbor, we found it surprisingly robust and most of our simulations led to the same result.

Figure 8 shows the time evolution of several resonant angles and eccentricities for **Set#1**. The first four plots on the left frame show $\sigma_1 = 3\lambda_{i+1} - 2\lambda_i - \varpi_i$ (in blue) and $\sigma_2 = 3\lambda_{i+1} - 2\lambda_i - \varpi_{i+1}$ (in red) for the first four inner planetary pairs (i.e. $i = 1, 2, 3, 4$). The inlaid box in the upper-right corners of each frame shows the planets involved in each case. All four pairs evolve towards an ACR (see, e.g., Beaugé et al. 2003; Michtchenko et al. 2006) characterized by equilibrium values $(\sigma_1, \sigma_2) = (0, \pi)$. As each link of the resonance chain falls into place the resonant angles and eccentricities (right frame in the figure) suffer a temporary kick, but are rapidly restored to low-amplitude oscillations around their stationary solutions.

The lower center plot shows the resonant angles of the 3/1 MMR between m_f and m_g . The capture of the pair into the two-planet resonance is only accompanied by a libration of $\theta_2 = 3\lambda_g - \lambda_f - \varpi_f - \varpi_g$ while all other possible resonant angles circulate. At the same time the outer pair enters the 3/1 commensurability, the outer triplet is captured in the $(2, -4, 3)$ 3P-MMR. The green data points in the lower-right plot show the time evolution of the resonant angle $\theta_{243} = 2\lambda_e - 4\lambda_f + 3\lambda_g - \varpi_g$ displaying an asymmetric libration during the time interval up to ~ 375 kyrs. All other possible resonant angles circulate.

It is difficult to prove that the capture in the three-planet resonance is a consequence of the trapping of the individual pairs in the 2-planet commensurabilities; the fact that the system chose the first-order 3P-MMR over its zero-order neighbor is intriguing; additional work is necessary before establishing in detail how this stable configuration is reached.

In order to test the stability of such a multi-resonant configuration, we introduced a smooth reduction in the surface density of the disk during a time interval centered around 375 kyrs and which lasted about ten thousand years. The subsequent evolution of the system occurs without the effects of disk damping. The librations of both the 3/1 MMR and the three-body resonance angles turn towards symmetric solutions as the surface density of the disk tends to zero, with $\theta_2 \rightarrow 0$ and $\theta_{243} \rightarrow \pi$. The orbital evolution of the full 6-planet resonance chain remains stable throughout the simulation with no indication of any incipient increase in am-

plitudes that could signal a future disruption of the system.

5.3. Tidal Evolution of the 6-Planet Chain

While we have succeeded in trapping the outermost triplet in the $(2, -4, 3)$ 3P-MMR and thus constructing a full 6-planet resonance chain, the offsets with respect to the nominal 2-planet resonances are much lower than observed. This is particularly notorious in the case of n_f/n_g whose current value ($\simeq 3.29$) is so distant from the exact resonance that it does not appear related.

The rest of the planetary pairs are also significantly displaced from the exact 3/2 resonance, with observed mean-motion ratios equal to 1.513, 1.518, 1.529 and 1.544, respectively. None of our capture simulations were able to obtain similar values, regardless of the chosen planetary masses or disk parameters. Consequently, if our previous results are representative of the primordial system, the current resonant offsets must have originated after the dissipation of the primordial disk; tidal effects with the central star appears as the only possible mechanism.

Several studies have analyzed how tidally-induced orbital variation generated in an inner planet may propagate to outer companions where tidal direct effects with the central star are negligible. In the case of secular (non-resonant) systems, this synergy affects mainly the eccentricities, although the finite equilibrium eccentricity induced by the mutual gravitational interactions also affects the rate of semi-major axis decay (e.g., Rodríguez et al. 2011; Greenberg & Van Laerhoven 2011). The case of resonant configurations, particularly involving 3-planet systems, is more intricate. Even though tidal evolution generates divergent migration and, thus, escape from 2-planet resonances, Papaloizou (2015) found that in the case 3 planets in a double resonance the escape occurs along a 3P-MMR commensurability. Similar results were reported by Charalambous et al. (2018) under a wide range of initial conditions and migration rates.

The offset observed in several planetary systems with respect to 2P-MMRs (e.g. Kepler-80, TOI-178) appear consistent with such an evolutionary route (e.g., MacDonald et al. 2016; Leleu et al. 2021), perhaps indicating that the resonant structure of small-mass planetary systems could have a stronger correlation to 3P-MMRs than to two-planet commensurabilities (Cerioni et al. 2022). However, in no case was a capture reported in a first-order three-planet resonance, nor was such a configuration suggested as an evolutionary route due to tidal effects.

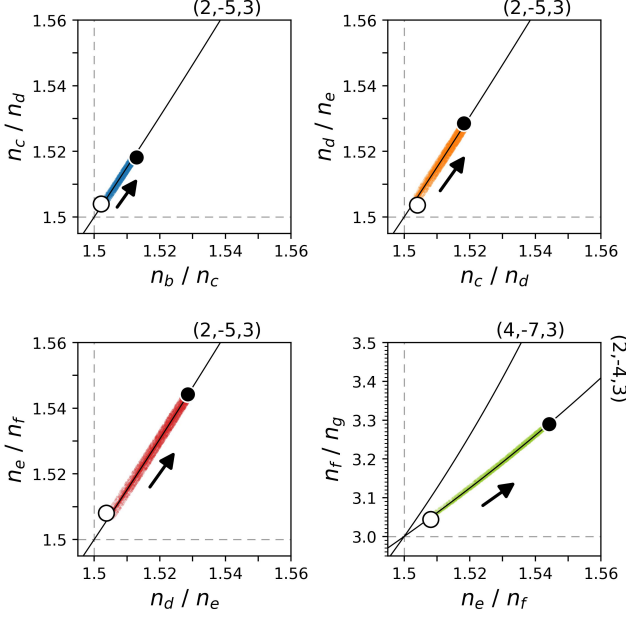


Figure 9. Tidal evolution of the K2-138 system in the mean-motion ratio plane. Colored lines correspond to the triplets of **Set#1**. Initial positions (white circles) correspond to the final stage of the capture simulation discussed in the previous section, with semi-major axes scaled to the observed system. The current mean-motion ratios of the planets are shown in black circles. Analogous results are obtained for **Set#2**.

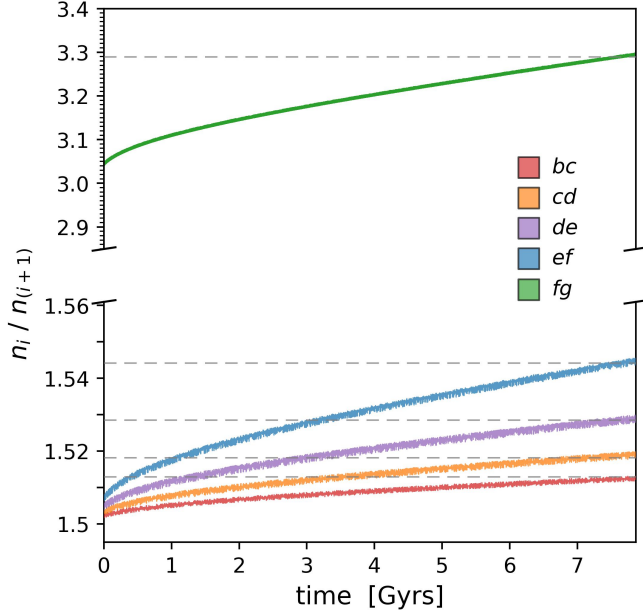


Figure 10. Time evolution of the mean-motion ratios of adjacent planets due to tidal interactions with the central star. As with the previous plot, initial conditions correspond to the final stage of the capture simulation of **Set#1**. Observed values are highlighted with horizontal dashed lines.

In order to check such a hypothesis for K2-138, we performed a series of N-body simulations of **Set#1** and **Set#2** under the combined effects of mutual gravitational perturbations and tides. The initial conditions were taken equal to the end product of the capture simulations, scaling the semi-major axes to better fit the observed system. Eccentricities and angles were untouched.

The tidal evolution was simulated following (Mignard 1979). This model considers tidal bulges raised on the planets as well as on the central star, which will be slightly delayed from (or ahead of) their instantaneous equipotential positions by a constant time-lag (CTL). We assumed a stellar tidal parameter $Q'_0 = 10^6$, while for the planets we chose $Q'_i = 10^2$, regardless of the body's mass or initial orbit. Recall that in the CTL model these numerical values are defined at the onset of the simulation and change during the orbital evolution of the system such that $Q'_i n_i = \text{const}$.

Figure 9 shows results for **Set#1**; analogous outcomes were obtained for **Set#2**. Each plot shows the evolutionary tracks of mean-motion ratios associated to adjacent planetary triplets. Initial values are depicted with white circles while the evolution of the system in these planes is shown with colored lines; arrows are drawn to help visualize the direction of the evolution. As expected, tidal effects increase the 2-planet resonance offset while preserving each triplet in its three-planet commensurability. This effect is also noted in the case of the outer triplet where the guiding route is the first-order 3P-MMR characterized by the index array $(2, -4, 3)$. Finally, the current mean-motion ratios of the planets are identified with black circles.

While not explicitly shown, semi-major axes decrease due to the tidal interactions, and this effect is strongest for the innermost planet. This differential migration pulls open the first planetary pair, which in turn opens up every other pair in the resonance chain, much like the motion of a pantograph-like mechanism. This is what is driving the evolution shown in Figure 9. More details will be given in Section 6. We can thus see that the observed values can in fact be obtained with tidal evolution, and that this mechanism is effective even in the case of the outer pair n_f/n_g .

Additional proof is given in Figure 10 which shows the evolution of each mean-motion ratio over time; current values are highlighted with horizontal dashed lines. Not only is the observed orbital separation consistent with the tidal evolution of the system, but the individual offsets of all planetary pairs are attained at the same time.

In these simulations, and for the adopted values of the tidal parameters, the current state of the system was

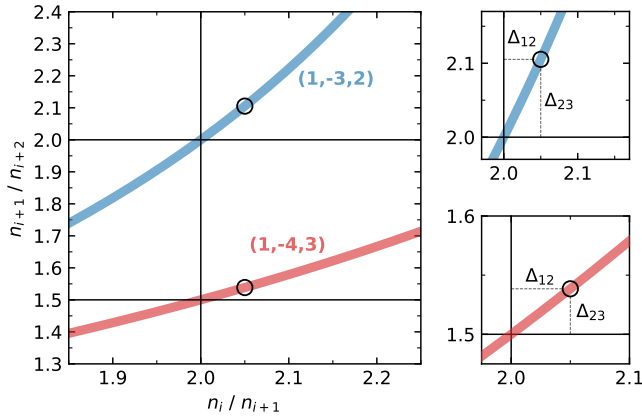


Figure 11. Sketch of two 3P-MMRs in mean-motion ratio space. Points correspond to triplets locked in the respective three-body resonances. **Right frames** are zoomed in with equal-scale axes, in order to better compare the slope of each curve, which determines the ordering of the two-body resonant offsets: $\Delta_{12} < \Delta_{23}$ for the blue curve and $\Delta_{12} > \Delta_{23}$ for the red.

reached at approximately 8 Gyrs after the dissipation of the primordial disk. Stellar age estimated from spectral analysis yields $T_{\text{age}} = 2.3^{+0.44}_{-0.36}$ Gyrs (Lopez et al. 2019). This requires a faster tidal evolution and thus a smaller value of Q'_i for the planets; we find that tidal parameters of the order of $Q'_i \simeq 30$ would have led to the same configuration in integration times consistent with T_{age} . However, stellar ages are notoriously difficult to evaluate with precision, and the actual value for this system could be larger.

6. THE PANTOGRAPHIC EFFECT

We repeated the previous simulations ignoring tidal interactions between the star and all but the innermost planet (m_b); results were indistinguishable, indicating that any change in the resonant offsets is mainly driven by the gravitational interactions with the other bodies and not by direct tidal forces. Thus, the current offsets of K2-138 may be used to estimate the tidal parameter of the inner planet but not of the rest of the system.

The observed increase of the resonance offsets with the semi-major axis is not a consequence of tidal interactions but of interplay between planets in a resonance chain. In order to understand the reason behind this effect, let us concentrate on a generic triplet m_1 , m_2 , and m_3 trapped in a double resonance but slightly away from the nominal commensurabilities:

$$\frac{n_1}{n_2} = \frac{p_1 + q_1}{p_1} + \Delta_{12} \quad ; \quad \frac{n_2}{n_3} = \frac{p_2 + q_2}{p_2} + \Delta_{23} \quad (8)$$

where Δ_{12} and Δ_{23} are the offsets initially determined by the capture process. Additionally, we assume that

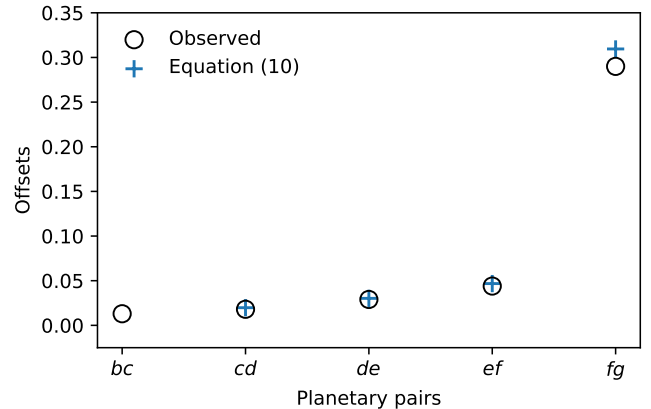


Figure 12. Open black circles plot the observed two-planet resonance offsets for the K2-138 system. Blue crosses show the predictions given by expression (10) assuming the current Δ_{bc} as a starting value.

the three planets are also trapped in a (k_1, k_2, k_3) three-body commensurability with no noticeable offset, such that

$$k_1 n_1 + k_2 n_2 + k_3 n_3 = 0. \quad (9)$$

where the order of the 3P-MMR is given by the sum of indexes $k_1 + k_2 + k_3$. Dividing equation (9) by n_2 and replacing equation (8), we get a condition for the offsets Δ_{12} and Δ_{23} that must be satisfied in the face of 2P- and 3P-MMRs:

$$\Delta_{23} = -k_3 \left(k_2 + k_1 \frac{p_1 + q_1}{p_1} + k_1 \Delta_{12} \right)^{-1} - \frac{p_2 + q_2}{p_2}. \quad (10)$$

Expression 10 shows that the offset of the outer pair, apart from being precisely determined by the first, can also be either smaller or higher than it, depending on the resonances involved. The same result can be deduced from analyzing 3P-MMR slopes in the mean-motion ratio plane, as the offsets will be the triplet's coordinates with the origin placed at the 2P-MMR intersection.

Figure 11 shows two examples. A triplet trapped in the $(1, -4, 3)$ commensurability close to the $n_1/n_2 = 2/1$ and $n_2/n_3 = 3/2$ will have $\partial(n_2/n_3)/\partial(n_1/n_2) < 1$ and thus the offset of the outer pair will be smaller than that of the inner pair. The opposite behavior is observed in the case of the three planets trapped in the $(1, -3, 2)$ 3P-MMR. In such a configuration the outer pair will suffer a larger departure from the nominal two-planet resonance even if m_1 is the only body driving the migration process.

The same principle can be applied to any number of interacting triplets in a long resonance chain, such as K2-138, where the $(2, -5, 3)$ and $(2, -4, 3)$ 3P-MMRs have slopes > 1 and the offsets increase with semi-major axis.

Furthermore, Expression 10 shows that only one given offset will determine the rest, and that if any planetary pair is spread apart or brought together, every other pair will simultaneously follow, while the triplets travel over the curves of 3-planet resonances. This linked motion holds a resemblance to the crossing points in a *pantograph*-like mechanism, and is what happens in Figure 9 when tidal effects bring the innermost planet inwards, pulling open the first planetary pair.

Figure 12 shows, in blue crosses, the observed offsets for each planetary pair. As mentioned previously, the values grow with the distance to the star with a surprisingly large jump in the case of Δ_{fg} due to the pronounced slope of the (2,-4,3) resonance. The open black circles show the values predicted from Equation (10) starting from the observed value of Δ_{bc} . The agreement with the real values is excellent in the case of the first three links, while some discrepancy is noted in the case of the outer pair. This difference is due to the accumulation of short-period deviations in each successive pair of planets.

7. DISCUSSION

In this paper we analyzed the current dynamical configuration of the complete K2-138 system. While the resonance chain involving the five innermost planets (m_b up to m_f) is an expected outcome of planetary migration, the orbital characteristics of the outer planet m_g are intriguing. Its large distance from the rest and apparent non-resonant dynamics strike out in such an otherwise compact system.

We analyzed two possible solutions to explain the dynamics of m_g . In the first, a small-mass outermost planet could have migrated slower than the inner system and become detached as the planets migrated closer to the star. This requires a small mass for m_g as well as fine-tuned initial separations and disk parameters. While possible, this formation scenario appears unlikely.

A second, and more interesting, explanation arose when noting that the three outer planets seem very close to the (2, -4, 3) first-order 3P-MMR. At first glance this proximity did not appear relevant given that these resonances are generally believed to be weak. Moreover, the mean-motion ratio $n_f/n_g \simeq 3.3$ appears too far from any significant 2-planet commensurability, thus making any correlation between the current separation and a past resonance capture very unlikely. A closer look, however,

showed both beliefs unfounded. A more massive outer planet with $m_g \gtrsim 9m_\oplus$ initially located beyond the 3/1 MMR with m_f could be trapped in a double resonance $(n_e/n_f, n_f/n_g) = (3/2, 3/1)$ leading to a libration of the critical angle of the 3P-MMR (2, -4, 3). This outcome was found for a wide range of initial conditions and disk parameters. The resulting configuration at the time of the dissipation of the primordial disk was composed of all 6 planets in a stable resonance chain with small offsets.

Tidal evolution of the system for times comparable with the system's age proved sufficient to convert the small resonance offsets to their present-day values, at least for values of Q' of the order of $Q'_b \simeq 30$ for the innermost planet. Direct tidal interactions between the other planets and the star proved negligible and thus their tidal parameters could not be constrained. Surprisingly even the current offset of the outer pair $n_f/n_g \simeq 3.3$ can be explained by tidal evolution alone, indicating that perhaps other seemingly non-resonant systems may be dynamically affected by two-planet or three-planet commensurabilities, even more so than previously thought (e.g., Cerioni et al. 2022).

The propagation of resonance offsets among members of a resonance chain can take several forms, depending on the 2P-MMRs and 3P-MMRs involved in each link. As a result, offset-inducing mechanisms such as tidal effects will not produce offsets that necessarily decrease with the distance from the star, as previously thought. Offsets among chained planets will also be linked such that the opening (contraction) of any single pair will simultaneously spread apart (bring together) the rest, a behavior reminiscent of the extension/contraction of a pantograph.

While at present it is not possible to prove that K2-138 forms a complete 6-planet resonant chain, including a first-order 3P-MMR, we believe the dynamical evidence is sufficient for such a claim to be at least very plausible.

ACKNOWLEDGMENTS

The authors would like to express their gratitude to the computing facilities of the Instituto de Astronomía Teórica y Experimental (IATE) and the Universidad Nacional de Córdoba (UNC). This work was funded by research grants from the Consejo Nacional de Investigaciones Científicas y Técnicas (CONICET) and the Secretaría de Ciencia y Tecnología (SECYT/UNC).

REFERENCES

- Batygin, K. 2015, MNRAS, 451, 2589, doi: 10.1093/mnras/stv1063
- Beaugé, C., & Cerioni, M. 2022, Celestial Mechanics and Dynamical Astronomy, 134, 57, doi: 10.1007/s10569-022-10113-4

- Beaugé, C., Ferraz-Mello, S., & Michtchenko, T. A. 2003, *ApJ*, 593, 1124, doi: [10.1086/376568](https://doi.org/10.1086/376568)
- Beaugé, C., Michtchenko, T. A., & Ferraz-Mello, S. 2006, *MNRAS*, 365, 1160, doi: [10.1111/j.1365-2966.2005.09779.x](https://doi.org/10.1111/j.1365-2966.2005.09779.x)
- Bulirsch, R., & Stoer, J. 1966, *Numerische Mathematik*, 8, 1, doi: [10.1007/bf02165234](https://doi.org/10.1007/bf02165234)
- Cerioni, M., Beaugé, C., & Gallardo, T. 2022, *MNRAS*, 513, 541, doi: [10.1093/mnras/stac876](https://doi.org/10.1093/mnras/stac876)
- Charalambous, C., Martí, J. G., Beaugé, C., & Ramos, X. S. 2018, *MNRAS*, 477, 1414, doi: [10.1093/mnras/sty676](https://doi.org/10.1093/mnras/sty676)
- Christiansen, J. L., Crossfield, I. J. M., Barentsen, G., et al. 2018, *AJ*, 155, 57, doi: [10.3847/1538-3881/aa9be0](https://doi.org/10.3847/1538-3881/aa9be0)
- Cresswell, P., & Nelson, R. P. 2006, *A&A*, 450, 833, doi: [10.1051/0004-6361/20054551](https://doi.org/10.1051/0004-6361/20054551)
- Delisle, J. B., & Laskar, J. 2014, *A&A*, 570, L7, doi: [10.1051/0004-6361/201424227](https://doi.org/10.1051/0004-6361/201424227)
- Goldreich, P., & Schlichting, H. E. 2014, *AJ*, 147, 32, doi: [10.1088/0004-6256/147/2/32](https://doi.org/10.1088/0004-6256/147/2/32)
- Goldreich, P., & Tremaine, S. 1980, *ApJ*, 241, 425, doi: [10.1086/158356](https://doi.org/10.1086/158356)
- Greenberg, R., & Van Laerhoven, C. 2011, *ApJ*, 733, 8, doi: [10.1088/0004-637X/733/1/8](https://doi.org/10.1088/0004-637X/733/1/8)
- Hardegree-Ullman, K. K., Christiansen, J. L., Ciardi, D. R., et al. 2021, *AJ*, 161, 219, doi: [10.3847/1538-3881/abeab0](https://doi.org/10.3847/1538-3881/abeab0)
- Henrard, J., & Lemaître, A. 1983, *Celestial Mechanics*, 30, 197, doi: [10.1007/BF01234306](https://doi.org/10.1007/BF01234306)
- Izidoro, A., Ogihara, M., Raymond, S. N., et al. 2017, *MNRAS*, 470, 1750, doi: [10.1093/mnras/stx1232](https://doi.org/10.1093/mnras/stx1232)
- Lee, M. H., & Peale, S. J. 2002, *ApJ*, 567, 596, doi: [10.1086/338504](https://doi.org/10.1086/338504)
- Lega, E., Morbidelli, A., & Nesvorný, D. 2013, *MNRAS*, 431, 3494, doi: [10.1093/mnras/stt431](https://doi.org/10.1093/mnras/stt431)
- Leleu, A., Alibert, Y., Hara, N. C., et al. 2021, *A&A*, 649, A26, doi: [10.1051/0004-6361/202039767](https://doi.org/10.1051/0004-6361/202039767)
- Lissauer, J. J., Ragozzine, D., Fabrycky, D. C., et al. 2011, *ApJS*, 197, 8, doi: [10.1088/0067-0049/197/1/8](https://doi.org/10.1088/0067-0049/197/1/8)
- Lithwick, Y., & Wu, Y. 2012, *ApJL*, 756, L11, doi: [10.1088/2041-8205/756/1/L11](https://doi.org/10.1088/2041-8205/756/1/L11)
- Lopez, T. A., Barros, S. C. C., Santerne, A., et al. 2019, *A&A*, 631, A90, doi: [10.1051/0004-6361/201936267](https://doi.org/10.1051/0004-6361/201936267)
- MacDonald, M. G., Ragozzine, D., Fabrycky, D. C., et al. 2016, *AJ*, 152, 105, doi: [10.3847/0004-6256/152/4/105](https://doi.org/10.3847/0004-6256/152/4/105)
- Malhotra, R. 1991, *Icarus*, 94, 399, doi: [10.1016/0019-1035\(91\)90237-N](https://doi.org/10.1016/0019-1035(91)90237-N)
- Michtchenko, T. A., Beaugé, C., & Ferraz-Mello, S. 2006, *Celestial Mechanics and Dynamical Astronomy*, 94, 411, doi: [10.1007/s10569-006-9009-x](https://doi.org/10.1007/s10569-006-9009-x)
- Mignard, F. 1979, *Moon and Planets*, 20, 301, doi: [10.1007/BF00907581](https://doi.org/10.1007/BF00907581)
- Papaloizou, J. C. B. 2015, *International Journal of Astrobiology*, 14, 291, doi: [10.1017/S1473550414000147](https://doi.org/10.1017/S1473550414000147)
- Ramos, X. S., Charalambous, C., Benítez-Llambay, P., & Beaugé, C. 2017, *A&A*, 602, A101, doi: [10.1051/0004-6361/201629642](https://doi.org/10.1051/0004-6361/201629642)
- Rodríguez, A., Ferraz-Mello, S., Michtchenko, T. A., Beaugé, C., & Miloni, O. 2011, *MNRAS*, 415, 2349, doi: [10.1111/j.1365-2966.2011.18861.x](https://doi.org/10.1111/j.1365-2966.2011.18861.x)
- Tanaka, H., Takeuchi, T., & Ward, W. R. 2002, *ApJ*, 565, 1257, doi: [10.1086/324713](https://doi.org/10.1086/324713)
- Tanaka, H., & Ward, W. R. 2004, *ApJ*, 602, 388, doi: [10.1086/380992](https://doi.org/10.1086/380992)
- Thommes, E. W., Bryden, G., Wu, Y., & Rasio, F. A. 2008, *ApJ*, 675, 1538, doi: [10.1086/525244](https://doi.org/10.1086/525244)
- Winn, J. N., & Fabrycky, D. C. 2015, *ARA&A*, 53, 409, doi: [10.1146/annurev-astro-082214-122246](https://doi.org/10.1146/annurev-astro-082214-122246)